



# An insight into crystal morphology-dependent catalytic properties of MOR-type titanosilicate in liquid-phase selective oxidation



Yulin Yang<sup>a</sup>, Jianghong Ding<sup>a</sup>, Chunhui Xu<sup>b</sup>, Weidong Zhu<sup>b</sup>, Peng Wu<sup>a,\*</sup>

<sup>a</sup> Shanghai Key Laboratory of Green Chemistry and Chemical Processes, Department of Chemistry, East China Normal University, North Zhongshan Rd. 3663, Shanghai 200062, PR China

<sup>b</sup> Key Laboratory of the Ministry of Education for Advanced Catalysis Materials, Institute of Physical Chemistry, Zhejiang Normal University, 321004 Jinhua, PR China

## ARTICLE INFO

### Article history:

Received 7 February 2015

Revised 27 February 2015

Accepted 2 March 2015

### Keywords:

Titanosilicate

Ti-MOR

Crystal morphology

Adsorption

Liquid-phase oxidation

Ammonoximation

Hydroxylation

## ABSTRACT

Mordenite zeolites, with controllable crystal morphologies grown orientedly along the *c*-axis, that is, the running direction of the 12-membered ring main channels, were hydrothermally synthesized. Corresponding Ti-containing mordenite (Ti-MOR) catalysts were then prepared by a secondary isomorphous substitution technique, which combined together acid-assisted dealumination and sequential TiCl<sub>4</sub> vapor treatment. The diffusion properties of this obtained Ti-MOR catalysts with various morphologies were measured using *n*-butane as a probe molecule, and their catalytic properties were investigated in the liquid-phase oxidation reactions including ketone ammoximation and aromatics hydroxylation. The mordenite zeolites with smaller crystals, especially consisting of nanoparticles, were in favor of forming tetrahedrally coordinated Ti in TiCl<sub>4</sub> vapor treatment. The physicochemical properties and catalytic activity of Ti-MOR exhibited regular changes with an increasing crystal length along the *c*-axis. The aromatic hydroxylation was more sensitive than ketone ammoximation to the variety of crystal length. In particular, the adsorption capacity ( $Q_{\infty}$ ), apparent diffusivity ( $D/L^2$ ), turnover number of ammoximation at 2.5 h and hydroxylation at 7 h decreased from 0.78 mmol g<sup>-1</sup>,  $22.7 \times 10^{-3} \text{ s}^{-1}$ , 1783 mol (Ti-mol)<sup>-1</sup> and 70.5 mol (Ti-mol)<sup>-1</sup> to 0.59 mmol g<sup>-1</sup>,  $4.2 \times 10^{-3} \text{ s}^{-1}$ , 500 mol (Ti-mol)<sup>-1</sup> and 3.4 mol (Ti-mol)<sup>-1</sup>, respectively, when the crystal size of Ti-MOR was enlarged from 110 to 5160 nm. The adsorption properties and oxidation activity of Ti-MOR were found to exhibit a distinct change around a crystal length demarcation of ca. 1 μm. Further studies indicated that the oxidation activity of Ti-MOR was proportional to its apparent diffusivity.

© 2015 Elsevier Inc. All rights reserved.

## 1. Introduction

Titanosilicates, typically represented by TS-1, have attracted enormous research interests because of their outstanding catalytic properties in liquid-phase selective oxidation reactions using hydrogen peroxide as a mild oxidant [1–3]. In the past decades, in addition to TS-1, dozens of Ti-containing porous materials with different structures and pore sizes have been developed, for example, Ti-MWW [4,5], Ti-Beta [6], Ti-MOR [7], Ti-MCM-41 [8], and Ti-SBA-15 [9]. Based on extensive fundamental researches, some titanosilicates have also achieved great successes in environmentally benign petrochemical processes in industry, for example, TS-1 for phenol hydroxylation [10], cyclohexanone ammoximation [11–13] and propylene epoxidation [14], and Ti-MWW for the ammoximation of methyl ethyl ketone [15].

Among the titanosilicates developed so far, Ti-MOR cannot yet be prepared directly by hydrothermal synthesis, but it is post-synthesized readily by isomorphous substitution of Ti ions into dealuminated mordenite through solid–gas reaction with TiCl<sub>4</sub> vapor [7]. With this secondary synthesis technique, Ti-MOR is prepared without using expensive organic structure-directing agents. Moreover, its large porosity of 12-membered ring (MR) endows Ti-MOR with attractive catalytic performances in ketone (or acetaldehyde) ammoximation and aromatics hydroxylation [16–21]. Previous researches focused mainly on the oxidation reactions themselves or the chemistry of Ti active sites. However, the relevance of diffusion properties and oxidation activity to the morphology and channel system of Ti-MOR has never been investigated in detail.

MOR framework is consisting of parallel 12-MR (6.5 × 7.0 Å) and 8-MR (2.6 × 5.7 Å) channels along *c*-axis, which are interconnected by 8-MR windows (3.4 × 4.8 Å) along *b*-axis [22,23]. Because of the small pore size of 8-MR channels and their bad

\* Corresponding author. Fax: +86 21 6223 2292.

E-mail address: [pwu@chem.ecnu.edu.cn](mailto:pwu@chem.ecnu.edu.cn) (P. Wu).

accessibility along *c*-axis, the MOR structure is commonly counted as one-dimensional 12-MR channel zeolite, which may induce diffusion limitations in its applications [23–25]. Up to now, the MOR aluminosilicates with different crystal morphologies and changeable crystal sizes have been synthesized, such as sphere-like, disk-like, needle-like, and nanosheet crystals [23,26,27]. All reported MOR zeolites seem to show an oriented growth along *c*-axis, the running direction of 12-MR channels.

Previous studies reveal that the properties and performances of zeolites in the applications of adsorption, separation, ion exchange, and heterogeneous catalysis strongly depended on their crystal morphology, including the shape and size [28,29]. The crystal morphology is anticipated to be closely related to the micropore accessibility and diffusion. As for titanosilicates, the diffusion and mass transfer are particularly important issues in the liquid-phase reactions using granular catalysts. TS-1 with a fine crystallite around 300 nm exhibited the best catalytic activity, but those with a crystal size exceeded 1  $\mu\text{m}$  or longer showed a significantly retarded activity because of diffusion problem [30,31]. It is thus preferable to synthesize nanoscaled titanosilicates in the pursuit of high performance.

Different to TS-1 equipped with a three-dimensional channel structure, the sole useful pore system of Ti-MOR is the 12-MR ( $6.5 \times 7.0 \text{ \AA}$ ) channel in *c*-axis direction. In the preparation of Ti-MOR, the  $\text{TiCl}_4$  (6.7  $\text{\AA}$ ) vapor molecules need to diffuse into the 12-MR channels firstly, and then they are incorporated into the framework. As for liquid-phase oxidation, the reactant molecules must approach to the Ti active sites located inside channels. Therefore, the crystal morphology of Ti-MOR may alter a double superimposition effect on the catalytic activity from the  $\text{TiCl}_4$  vapor treatment and the catalytic reaction. Nevertheless, how the crystal morphology influences the catalytic performance of Ti-MOR has not yet been investigated systematically.

In this study, a series of mordenite zeolites with different crystal morphologies, ranging from nanometer scale to micrometer, have been hydrothermally synthesized, and corresponding Ti-MOR catalysts were then post-synthesized. The crystal morphology-dependent physicochemical properties and catalytic performances have been investigated. The catalytic activity of Ti-MOR in liquid-phase oxidations was correlated to its crystal morphology, length as well as apparent diffusivity.

## 2. Experimental

### 2.1. Synthesis of MOR zeolites and dealuminated MOR with different morphologies

A couple of commercially available Na-mordenite zeolites with prism-like morphologies and different crystal lengths, denoted as M-2 (230 nm) and M-3 (630 nm), were used as received.

Na-mordenite M-1 sample with granular-like crystal shape was synthesized from colloidal silica (30.0 wt.%  $\text{SiO}_2$ , 0.3 wt.%  $\text{Na}_2\text{O}$ , 69.7 wt.%  $\text{H}_2\text{O}$ ), sodium hydroxide, sodium aluminate (44.39 wt.%  $\text{Al}_2\text{O}_3$ , 37.50 wt.%  $\text{Na}_2\text{O}$ ), and boric acid. These chemicals were mixed in distilled water under vigorous stirring, forming a homogeneous gel. Then, 0.5 wt.% M-3 zeolite, relative to the weight of  $\text{SiO}_2$  in gel, was added as the seed. The gel had a molar composition of 1.0  $\text{SiO}_2$ :0.24  $\text{Na}_2\text{O}$ :0.067  $\text{Al}_2\text{O}_3$ :22  $\text{H}_2\text{O}$ :0.2  $\text{H}_3\text{BO}_3$ . After being stirred at room temperature for 2 h, the resultant gels were transferred into a Teflon-lined stainless steel autoclave, which was tumbled at 60 rpm and at 443 K for 24 h.

M-4 sample with needle-like shape was synthesized by two steps. In a typical run, 7.65 g piperidine (PI), 0.15 g sodium hydroxide, 0.48 g sodium aluminate, and 20 g colloidal silica were firstly mixed in order into 22 g distilled water under vigorous stirring

for 2 h, forming gel A with a molar composition of 1.0  $\text{SiO}_2$ :0.9 PI:0.05  $\text{Na}_2\text{O}$ :0.025  $\text{Al}_2\text{O}_3$ :20  $\text{H}_2\text{O}$ . The gel A was tumbled in a Teflon-lined stainless steel autoclave at 60 rpm and at 423 K for 24 h. Solution B was prepared by dissolving 1.06 g sodium hydroxide and 0.96 g sodium aluminate in 36 g distilled water. After the crystallization of solution A for 24 h, the autoclave was cooled, and solution B was added under vigorous stirring. Then 0.5 wt.% M-3, relative to the weight of  $\text{SiO}_2$  in gel A, was added as the seed. After stirring for 2 h at room temperature, the resultant gels were crystallized in an autoclave at 443 K for 48 h under tumbling (60 rpm).

The procedures and gel composition for synthesizing M-5, a sample with a fiber-like crystal shape, were the same as M-1 except that the silicon source was replaced by silica gel (95.0 wt.%  $\text{SiO}_2$ , 5.0 wt.%  $\text{H}_2\text{O}$ , Qingdao Haiyang Chemical Co., Ltd.), and the synthesis was carried out free of boric acid.

After completion of the crystallization, the autoclave was cooled and the solid product was obtained by filtrating, washing with water, and drying in air at 353 K for 12 h. All Na-mordenite zeolites were ion-exchanged with 1.0 M ammonium chloride at a solid-to-liquid ratio of 1:40 at 353 K for 2 h. The ion exchange repeated twice. The sample was subsequently washed with deionized water and calcined at 973 K for 10 h, giving rise to proton-type zeolites, H-MOR. The H-MOR samples were refluxed in 6 M  $\text{HNO}_3$  solution at a solid-to-liquid ratio of 1:50 for 10 h. The acid-treated samples were subsequently filtrated and washed with deionized water until the pH value of the filtrate was over 5. These procedures were repeated once more, giving rise to dealuminated zeolites, Del-MOR.

### 2.2. Preparation of Ti-MOR titanosilicates

Ti-containing mordenite was post-synthesized through a solid-gas reaction between dealuminated MOR and  $\text{TiCl}_4$  vapor at elevated temperature following previous procedures [7,18]. For a typical preparation, a Del-M sample (2.0 g) placed in a quartz tube reactor ( $\varnothing$  3 cm) was pretreated at 673 K for 2 h in a dry  $\text{N}_2$  stream (50  $\text{mL min}^{-1}$ ). Then,  $\text{TiCl}_4$  vapor was brought into the reactor by  $\text{N}_2$  flow, treating the Del-M sample at 673 K for 2 h. The sample was then purged with pure  $\text{N}_2$  at the same temperature for 1 h to remove any residual  $\text{TiCl}_4$  from the zeolite powder. After cooling to room temperature in  $\text{N}_2$  atmosphere, the treated samples were washed with deionized water and dried in air at 353 K overnight, resulting in Ti-M- $x$  ( $x = 1-5$ ).

### 2.3. Characterization methods

Powder X-ray diffraction (XRD) patterns were collected on a Rigaku Ultima IV diffractometer using  $\text{CuK}\alpha$  radiation ( $\lambda = 1.5405 \text{ \AA}$ ) at 35 kV and 25 mA in the  $2\theta$  angle range of 5–35°. Scanning electron microscopy (SEM) was performed on a Hitachi S-4800 microscope to determine the morphology. The  $^{29}\text{Si}$  MAS NMR spectra were measured on a VARIAN VNMRS 400WB NMR spectrometer using single-pulse method at a frequency of 79.43 MHz, a spinning rate of 3 kHz, and a recycling delay of 60 s. The chemical shift was referred to  $\text{Q}_8\text{M}_8$  ( $[(\text{CH}_3)_3\text{SiO}_8]\text{SiO}_{12}$ ). The Si, Ti, and Al contents were determined by inductively coupled plasma emission spectrometry (ICP) on a thermo IRIS Intrepid II XSP atomic emission spectrometer after dissolving the samples in HF solution. The specific surface area, pore volume, and pore size distribution were measured by  $\text{N}_2$  adsorption at 77 K on a BELSORP-MAX instrument after the samples were activated in advance at 573 K under vacuum for at least 4 h. The UV-visible diffuse reflectance spectra were recorded on a Shimadzu UV-2550 spectrophotometer using  $\text{BaSO}_4$  as a reference. The IR spectra were collected on Nicolet Nexus 670 FT-IR spectrometer in absorbance mode at a spectral resolution of  $2 \text{ cm}^{-1}$  using KBr technique

( $\varnothing$  1.5 cm wafer, 3 wt.% diluted in KBr). Thermogravimetry (TG) and derivative thermogravimetry (DTG) analyses were carried out on a Mettler TGA/SDTA 851<sup>e</sup> instrument with a ramping rate of 10 K min<sup>-1</sup> in an air flow of 40 mL min<sup>-1</sup>. The sorption of *n*-butane on various Ti-M samples was performed on a NETZSCH STA 449C thermogravimetric analyzer. The samples were pretreated at 623 K for 5 h in a helium stream (36 mL min<sup>-1</sup>). The dependence of adsorption amount on time was then recorded under a *n*-butane partial pressure of 10 kPa at 198 K.

#### 2.4. Catalytic reactions

The ammoxidation of cyclohexanone was carried out in a batchwise reactor using water as a solvent. The mixture of catalyst (25 mg), 10 mmol cyclohexanone, and 6 g H<sub>2</sub>O was heated in a 50-mL flask to 333 K, where H<sub>2</sub>O<sub>2</sub> (30 wt.%) and NH<sub>3</sub>·H<sub>2</sub>O were added to initiate the reaction for a desirable period of time (0.5–2.5 h). The molar ratio of NH<sub>3</sub>:H<sub>2</sub>O<sub>2</sub>:cyclohexanone was 1.5:1.2:1. The reusability of Ti-M samples in cyclohexanone ammoxidation was carried out with an enlarged catalyst loading of 0.1 g, and used catalyst was washed with water and acetone, and dried at 353 K. The ratio of catalyst:H<sub>2</sub>O:ketone:H<sub>2</sub>O<sub>2</sub>:NH<sub>3</sub> was kept at 0.1 g:6 g:10 mmol:12 mmol:15 mmol and reacted at 333 K for 2 h in a 50-mL flask. All catalysts were used five cycles.

In a typical run of toluene hydroxylation, the mixture of 50 mg catalyst, 10 g toluene, and 1 g H<sub>2</sub>O was stirred vigorously at 363 K. Then, 10 mmol H<sub>2</sub>O<sub>2</sub> (30 wt.%) was added into the reactor to start the hydroxylation. After the reaction was carried out for a desirable period of time (1–7 h), 20 mL ethanol was added to homogenize the organic phase and the aqueous phase.

After removing the catalyst solid, the products of two reactions were analyzed on a gas chromatograph (Shimadzu GC-2014) and quantified using chlorobenzene as an internal standard.

### 3. Results and discussion

#### 3.1. Synthesis and characterization of Na-MOR zeolite with different morphologies

Fig. 1 shows the XRD patterns of five Na-MOR samples with different morphologies. They were all of pure crystalline phases with the MOR topology, with other impurity unobserved. The intensity of the [002] reflection, related to the *c*-axis, showed no obvious difference for all samples. However, compared to the XRD patterns of M-1, M-2 and M-3, the intensities of [1 1 0], [0 2 0], [2 0 0], [3 1 0], [3 3 0], [1 5 0], and [3 5 0] reflections decreased distinctly for M-4

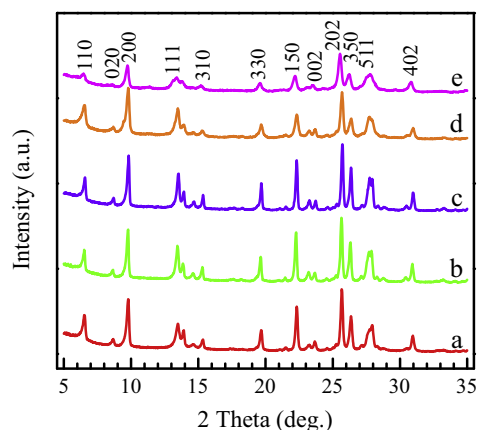


Fig. 1. XRD patterns of Na-MOR samples. (a) M-1, (b) M-2, (c) M-3, (d) M-4, and (e) M-5.

and M-5. The M-4 and M-5 samples also showed the phenomena of peak broadening in XRD patterns (Fig. 1d and e). This is probably resulted from the decreased crystal sizes along *a*-axis and *b*-axis directions, or the increased one along *c*-axis direction [21], as the reflections of MOR crystalline structure are mostly independent of the *c*-axis.

SEM micrographs shown in Fig. 2 exhibit that all MOR samples differed greatly in morphologies with each other. As summarized in Table 1, the crystal length was in the order of M-1 (110 nm) < M-2 (230 nm) < M-3 (630 nm) < M-4 (2450 nm) < M-5 (5160 nm). The aspect ratio, that is, length/width ratio, also varied significantly between different Na-MOR samples. In addition, the Si/Al ratio decreased with the crystal length enlarging.

Combining the information given by XRD patterns (Fig. 1) and SEM micrographs (Fig. 2), we can determine that the crystal length is along with the *c*-axis direction of MOR topology. Videlicet, the main 12-MR channels of MOR increase in length with the direction of crystal growth, as displayed in Scheme 1.

#### 3.2. Preparation and characterization of Ti-MOR with different morphologies

The structure of these mordenite samples after dealumination and Ti incorporation was first investigated with XRD (Supplementary Material, Fig. S1). All Ti-M samples were still characteristic of a typical MOR topology and possessed the diffractions very comparable to corresponding pristine Na-MOR in intensity. This indicated that there was no destruction of the crystalline structure.

To evaluate the porosity of Ti-M samples, the N<sub>2</sub> adsorption measurements were performed at 77 K. They exhibited type I adsorption-desorption isotherms and similar adsorption behavior at low relative pressure irrespective of the crystal morphology (Fig. 3). The specific surfaces calculated by Langmuir method were in a similar range of 555–595 m<sup>2</sup> g<sup>-1</sup> (Table 2), which confirmed that these samples were of highly crystalline. The differences observed in XRD intensity simply resulted from the oriented crystal growth along specific crystalline planes, that is, *c*-axis direction. Nevertheless, with respect to the adsorption behavior in the region of higher relative pressure, there were slight differences among the Ti-M samples. Compared to prism-like samples (Ti-M-2 and Ti-M-3), the other three samples all showed slightly enhanced N<sub>2</sub> adsorption at *P*/*P*<sub>0</sub> = 0.9–0.99 (Fig. 3). This is probably due to the nitrogen adsorption inside the intercrystal pores that existed in Ti-M-1 with a much smaller crystals (110 nm), as well as Ti-M-4 and Ti-M-5 with much longer crystals [2450–5160 nm].

Following previously well-established procedures [7], we conducted the incorporation of Ti ions into the defect sites such as hydroxyl nests in the MOR framework by atom-planting method using TiCl<sub>4</sub> vapor. The existing states of the Ti species introduced were first investigated by IR spectroscopy. Titanosilicates are characteristic of an IR band at approximately 960 cm<sup>-1</sup> irrespective of crystalline structure, which is taken as an important evidence for the presence of tetrahedral Ti species [2,3]. As shown in Fig. 4A, all Ti-MOR samples showed the typical band at 963 cm<sup>-1</sup>, which is attributed to the Si–O–Ti stretching vibration. The band intensity decreased with the crystal length increasing, especially when the crystal reached micrometer scale range, indicating the amount of incorporated Ti was reduced.

The level of dealumination was investigated by chemical analysis. As depicted in Table 2, when the crystal was within nanometer size, the Si/Al ratio was all over 200. However, with the crystal size up to micrometer, the Si/Al ratio was decreased to 112 and 156 for Ti-M-4 and Ti-M-5, respectively, implying that the dealumination process was affected by the crystal morphology. As the crystal length became larger, namely the length of 12-MR channels was

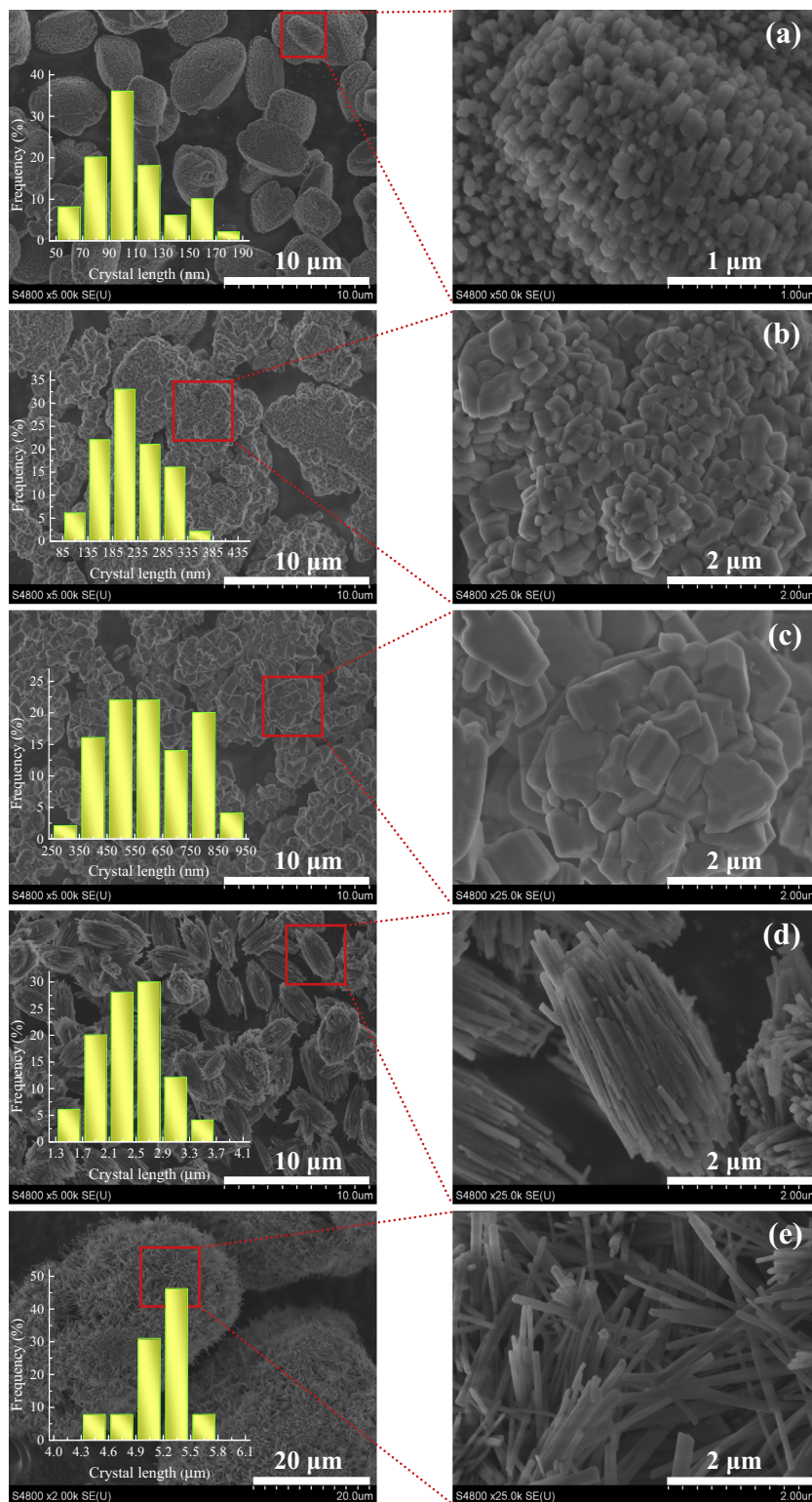


**Fig. 2.** SEM micrographs of Na-MOR samples. (a) M-1 (granular-like), (b) M-2 (prism-like), (c) M-3 (prism-like), (d) M-4 (needle-like), and (e) M-5 (fiber-like).

enlarged, the acid molecules needed to take a longer diffusion distance to enter into the 12-MR channels. This was same for the aluminum species diffusing out of the channels. Exceptionally, the crystals of Ti-M-5 were larger than that of Ti-M-4, but the former had a higher Si/Al ratio, that is, a relatively lower Al content. This could be a result of the different crystal aggregation degrees

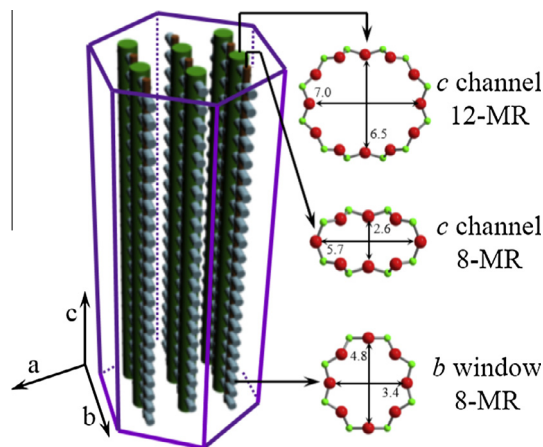
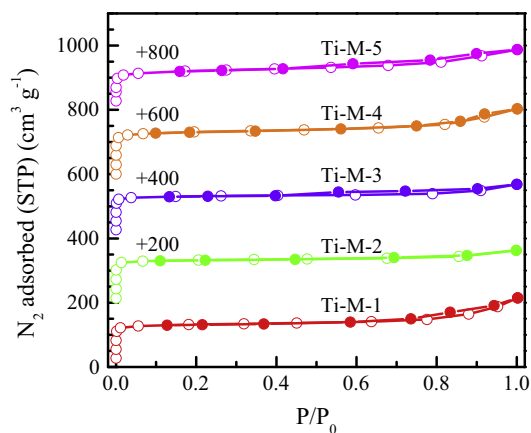
between these two materials. Compared with the M-5 crystals loosely piled up together (Fig. 2e), the M-4 particles were tightly bound together forming sarciniform aggregates (Fig. 2d), which induced a slightly more diffusing limitations than the former. The saturated amount of incorporated Ti, represented by Si/Ti ratio, varied obviously with the crystal length. The Si/Ti ratio was at a

**Table 1**  
Characterizations of various Na-MOR zeolites.

No.	Sample	Crystal length <sup>a</sup> (c, nm)	Crystal width <sup>a</sup> (a ≈ b, nm)	Aspect ratio (c/b)	Si/ Al <sup>b</sup>
1	M-1	110	70	1.6	6.1
2	M-2	230	150	1.5	6.5
3	M-3	630	350	1.8	6.6
4	M-4	2450	100	24.5	5.9
5	M-5	5160	100	51.6	4.7

<sup>a</sup> The crystal length and width in this table are an average of 50 appropriate crystals from SEM images.

<sup>b</sup> Molar ratio given by ICP analysis.

**Scheme 1.** Crystal morphology, channel network, and pore sizes of MOR zeolite.**Fig. 3.** N<sub>2</sub> adsorption–desorption isotherms of various Ti-M samples at 77 K.**Table 2**  
Physico-chemical properties of different Ti-M samples.

No.	Sample	Si/Al <sup>a</sup>	Si/Ti <sup>a</sup>	SA (m <sup>2</sup> g <sup>-1</sup> ) <sup>b</sup>	Q <sup>3</sup> /(Q <sup>3</sup> + Q <sup>4</sup> ) (%) <sup>c</sup>
1	Ti-M-1	429	73	595	1.7 (8.9) <sup>d</sup>
2	Ti-M-2	416	75	591	0.5 (3.1) <sup>d</sup>
3	Ti-M-3	234	77	582	1.5 (4.1) <sup>d</sup>
4	Ti-M-4	112	138	587	6.3 (9.3) <sup>d</sup>
5	Ti-M-5	156	116	555	12.7 (15.8) <sup>d</sup>

<sup>a</sup> Molar ratio given by ICP analysis.

<sup>b</sup> Specific surface area (Langmuir) given by N<sub>2</sub> adsorption at 77 K.

<sup>c</sup> Determined by <sup>29</sup>Si MAS NMR investigation.

<sup>d</sup> The figure between brackets represents the Q<sup>3</sup> content of corresponding dealuminated MOR sample (Del-M) respectively.

comparable level of 73–77, for Ti-M-1, Ti-M-2, and Ti-M-3 (Table 2, Nos. 1–3). However, the Si/Ti ratio increased to 138 and 116 for Ti-M-4 and Ti-M-5 both with the micrometer-sized crystals in length. The TiCl<sub>4</sub> vapor molecules with a relatively bulky dimension (6.7 Å) may suffer diffusion difficulty when entering into the 12-MR channels of mordenite. This kind of limitation is considered to be enhanced distinctly inside the channels with longer diffusion distance. Similar to the Si/Al ratio for Ti-M-4 and Ti-M-5, the Si/Ti ratio of Ti-M-4 was a little higher than Ti-M-5, of which the phenomenon was also caused by the aggregation of crystals.

UV–visible spectroscopy was employed to characterize further the coordination states of the Ti species incorporated. All Ti-M samples revealed a dominated band at approximately 210 nm (Fig. 4B), which is assigned to the ligand-to-metal charge transfer from O<sup>2-</sup> to Ti<sup>4+</sup>. This band is usually observed for a variety of Ti-substituted zeolites, and it is characteristic of tetrahedrally coordinated Ti highly dispersed in the framework [32]. Obviously, the intensity of 210 nm band decreased along with the crystal particle growing, in agreement with IR spectra. On the contrary, the intensity of 260 nm, assigned to hexa-coordinated Ti outside the framework, increased accompanied by the crystal particle expanding. Moreover, no obvious band was observed around 330 nm due to anatase phase for Ti-M-1, Ti-M-2, and Ti-M-3. The 330 nm band was observed visibly when the crystal length reached or exceeded 1 μm for Ti-M-4 and Ti-M-5. This is because that when suffering a stronger diffusion resistance in longer 12-MR channels, the TiCl<sub>4</sub> vapor molecules tended to form easily the hexa-coordinated Ti species and anatase phase in the extra-framework positions.

Based on the results of IR spectroscopy, UV–visible spectroscopy, and ICP analysis, it is concluded that the amount of tetrahedrally coordinated Ti dispersed in framework decreased with the increase of crystal length.

With respect to the Ti incorporation mechanism, we once addressed that the Ti species were inserted into the hydroxyl nests through the reaction of one TiCl<sub>4</sub> molecule with four internal silanol groups on the basis of isotope exchange with C<sup>18</sup>O<sub>2</sub> [7]. Here, <sup>29</sup>Si MAS NMR spectra were measured to take insight into this issue. As shown in Fig. 5, two main resonances were observed at –113 ppm and –115 ppm, which are attributed to the Q<sup>4</sup> groups in Si(SiO)<sub>4</sub> configuration [33]. With comparable intensities, they were caused by overlap of four crystallographically non-equivalent tetrahedral Si(SiO)<sub>4</sub> sites. The acid treatments removed the Al ions from the framework extensively and developed a broad resonance around –103 ppm, assigned to the Q<sup>3</sup> groups of silicon-bearing OH groups, Si(OH)(SiO)<sub>3</sub> [34]. According to the titaniation mechanism investigated previously [7], the quantity of Q<sup>3</sup> groups remaining after TiCl<sub>4</sub> treatment would reflect the level of titaniation. Compared to dealuminated samples (Del-M) (Fig. 5A), the resonance intensity of Q<sup>3</sup> groups at –103 ppm was decreased for corresponding Ti-M samples (Fig. 5B), especially for the Ti-M-1, Ti-M-2, and Ti-M-3 materials with nanosized crystals. A calculation of deconvoluted spectra showed that the Q<sup>3</sup> percentages were decreased by TiCl<sub>4</sub> vapor treatment from 8.9%, 3.1%, 4.1%, 9.3%, and 15.8% of Del-M-1, Del-M-2, Del-M-3, Del-M-4, and Del-M-5 to 1.7%, 0.5%, 1.5%, 6.3%, and 12.7% of Ti-M-1, Ti-M-2, Ti-M-3, Ti-M-4, and Ti-M-5, respectively (Table 2). It is worth noting that the Ti-M-1 had the biggest drop of Q<sup>3</sup> groups (7%), while the decline values of other four samples were about 3%. Moreover, even for the micrometer-scaled materials, Ti-M-4 and Ti-M-5, contained a much higher content of Q<sup>3</sup> than that of other samples, the TiCl<sub>4</sub> vapor treatment could only remove a small part of them. The result again confirmed that for the micrometer-sized crystals, the Ti species were difficult to be incorporated in the framework according to the titaniation mechanism through the reaction between the TiCl<sub>4</sub> vapor molecules and the Si–OH groups.

### 3.3. Molecular diffusion behaviors of various Ti-MOR zeolites

The diffusion properties of zeolites are frequently investigated by employing hydrocarbons as probe molecules [35]. Existing researches on the adsorption properties of mordenite are mainly focused on the lower availability of micropore volume resulted from the lodged  $\text{Na}^+$  cations [36,37] or octahedral non-framework alumina [24]. The influence of morphology on the diffusion performance of MOR-type zeolite has seldom been studied up to date. Fig. 6A shows the uptake curves of *n*-butane on different Ti-M

samples. The maximum uptake of Ti-M-1 was achieved after 5 min, roughly the same as Ti-M-2 and Ti-M-3. However, at least 10 min was required to reach the maximum uptake for Ti-M-4 and Ti-M-5. And, the adsorption capacity of Ti-M-1, Ti-M-2, and Ti-M-3 was 0.78, 0.77, and 0.76  $\text{mmol g}^{-1}$ , respectively (Table 3), difference of which was little. Nevertheless, the values of Ti-M-4 and Ti-M-5 decreased to 0.71 and 0.59  $\text{mmol g}^{-1}$ , respectively (Table 3). Thus, the adsorption capacity of Ti-M was negatively related to its crystal length in the order of Ti-M-1 > Ti-M-2 > Ti-M-3 > Ti-M-4 > Ti-M-5.

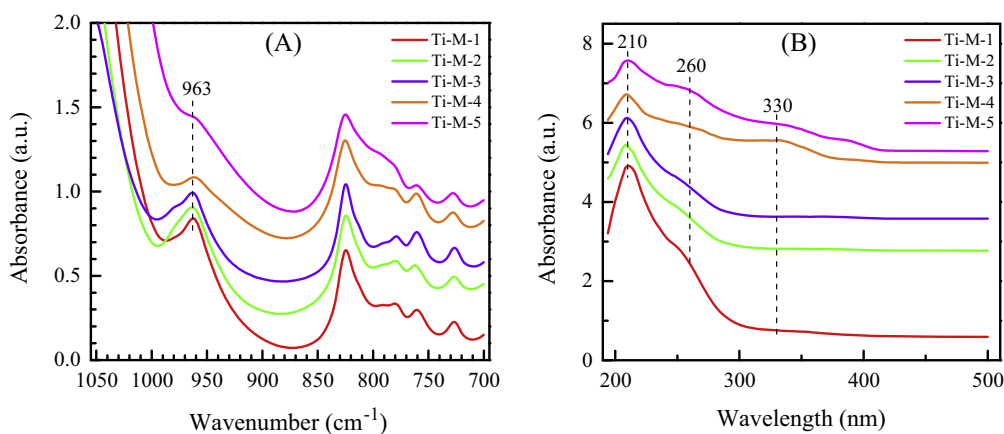


Fig. 4. IR spectra in the framework vibration region (A) and UV-visible spectra (B) of various Ti-M samples with different morphologies.

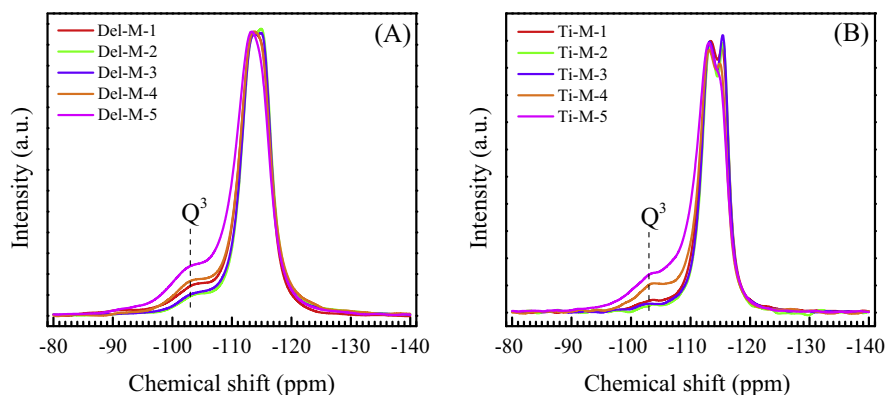


Fig. 5.  $^{29}\text{Si}$  MAS NMR spectra of various Del-M (A) and Ti-M (B) samples.

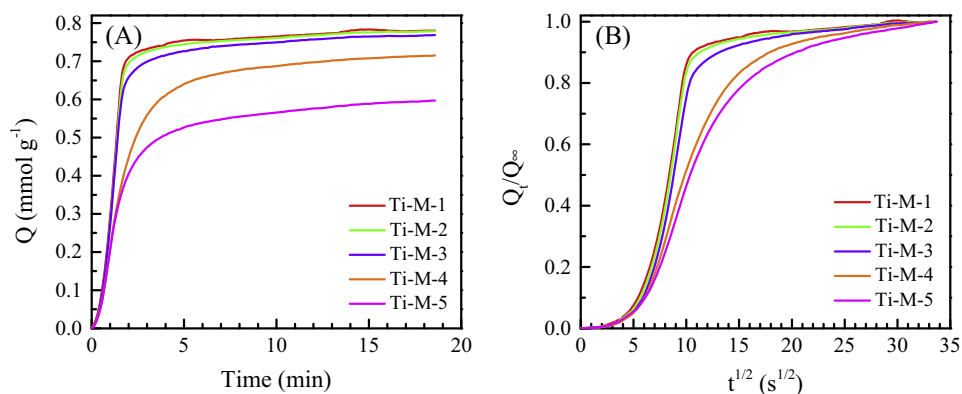


Fig. 6. *n*-Butane uptake curves (A) and relative adsorption uptake of *n*-butane (B) in various Ti-M samples. Sorption at 298 K and a *n*-butane partial pressure of 10 kPa.

**Table 3**

Adsorption capacity ( $Q_\infty$ ) and apparent diffusivity ( $D/L^2$ ) of *n*-butane adsorbed in different Ti-M samples.

Sample	Ti-M-1	Ti-M-2	Ti-M-3	Ti-M-4	Ti-M-5
$Q_\infty$ (mmol g <sup>-1</sup> )	0.78	0.77	0.76	0.71	0.59
$D/L^2$ (10 <sup>-3</sup> s <sup>-1</sup> )	22.7	20.1	17.7	5.8	4.2

Fig. 6B shows the dependence of the relative adsorption uptake on square root of time, where  $Q_t$  and  $Q_\infty$  denote the mass adsorbed at time  $t$  and infinite time, respectively. The  $Q_\infty$  value was taken from the saturated amount in each uptake curve. The diffusion rates of *n*-butane on various Ti-M samples also gave inverse correlations with their particle size. During the initial stage of uptake, the following appropriate solution applies [35]:

$$\frac{Q_t}{Q_\infty} = \frac{2}{\sqrt{\pi}} \sqrt{\frac{D}{L^2}} \sqrt{t}$$

where  $Q_t/Q_\infty$  is the normalized loading,  $D$  is the diffusivity,  $L$  is the characteristic diffusion length,  $D/L^2$  is the apparent diffusivity, and  $t$  is time. This fitting adequately describes the experimental data covering the uptake curve from  $Q_t/Q_\infty \sim 0.1$  up to  $Q_t/Q_\infty \sim 0.8$ . The  $D/L^2$  ratio of various Ti-MOR samples obtained according to the equation is compared in Table 3. It is obvious that the apparent diffusivity ( $D/L^2$ ) did not decrease significantly when the particle size of adsorbent (Ti-M) expanded within nanometer scale. However, when the particle size of Ti-M enlarged up to micrometer scale, the apparent diffusivity ( $D/L^2$ ) would fall sharply to  $4.2 \times 10^{-3} \text{ s}^{-1}$  (Ti-M-5, 5160 nm) from  $22.7 \times 10^{-3} \text{ s}^{-1}$  (Ti-M-1, 110 nm), with a decreasing degree of about fivefold. Thus, the value of 1  $\mu\text{m}$  for crystal length is a distinguished demarcation line determining the adsorption and diffusion properties of Ti-MOR zeolite.

### 3.4. Catalytic properties of various Ti-M zeolites in liquid-phase oxidations

#### 3.4.1. Ammoximation of cyclohexanone with ammonia and hydrogen peroxide

The influence of morphology on Ti-M catalytic performance was first demonstrated in the ammoximation of cyclohexanone with ammonia and hydrogen peroxide. The cyclohexanone oxime product is the raw material for producing  $\epsilon$ -caprolactam, an important intermediate for nylon-6 synthesis. In addition to TS-1 [38] and Ti-MWW [39], Ti-MOR also proves to be an efficient catalyst for this reaction [16].

**Table 4**

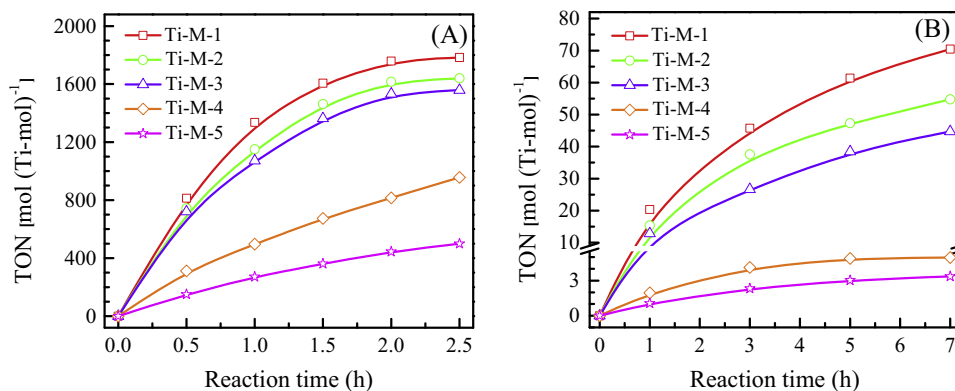
A comparison of cyclohexanone ammoximation on different Ti-M samples.<sup>a</sup>

No.	Sample	Cyclohexanone conv. (%)	Initial reaction rate (mmol g <sup>-1</sup> h <sup>-1</sup> )	Oxime sel. (%)
1	Ti-M-1	94.4	344.4	>98
2	Ti-M-2	87.3	316.8	>98
3	Ti-M-3	80.0	296.0	>98
4	Ti-M-4	27.0	70.4	>98
5	Ti-M-5	16.6	40.0	>98

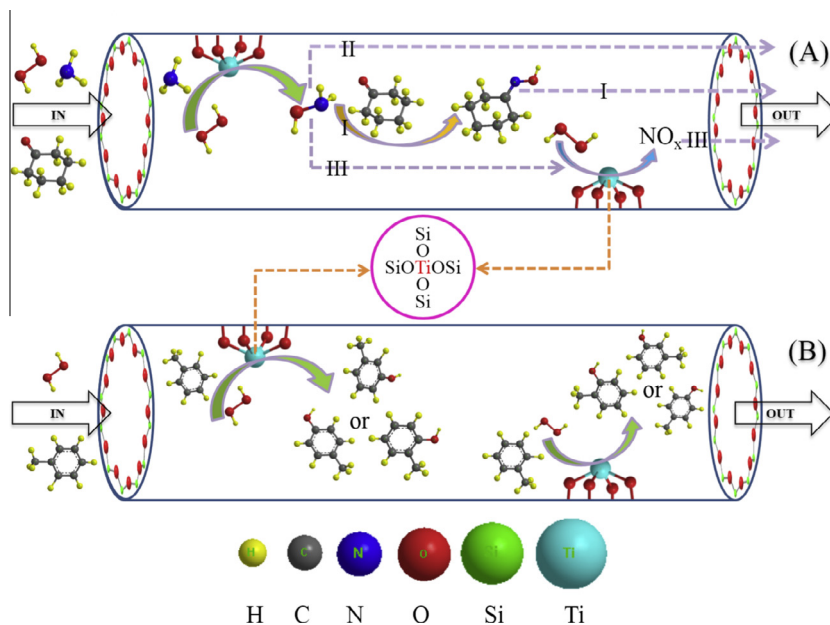
<sup>a</sup> For ammoximation conditions, see Fig. 8; reaction time, 2.5 h.

Fig. 7A shows the time course of specific activity per Ti site, that is, turnover number (TON). The TON of Ti-M-1, Ti-M-2, and Ti-M-3 increased rapidly with reaction time at initial stage, while the disparity among them was slight, and the initial reaction rate of each sample was 344.4, 316.8, and 296.0 mmol g<sup>-1</sup> h<sup>-1</sup>, respectively (Table 4, Nos. 1–3). As for Ti-M-4 and Ti-M-5, the TON increased slowly along with reaction time. Their initial reaction rate was lowered to 70.4 and 40.0 mmol g<sup>-1</sup> h<sup>-1</sup>, respectively (Table 4, Nos. 4 and 5). The difference in catalytic activity of TON was distinct between these two micrometer-sized samples and the other three nanosized ones. After 2.5 h, the reaction approximated the equilibrium, giving a cyclohexanone conversion of 94.4%, 87.3%, 80.0%, 27.0%, and 16.6% over Ti-M-1, Ti-M-2, Ti-M-3, Ti-M-4, and Ti-M-5, respectively, while with a high oxime selectivity over 98% for all samples (Table 4). Obviously, the catalysts of nanosized crystals (Ti-M-1, Ti-M-2, and Ti-M-3) were benefit for the ammoximation, showing a narrowed disparity in TON and reaction rate at initial stage. Accompanied by reaction time stretching, the gap of TON became larger, as well as the ketone conversion. More explicitly, when crystal particles reached the micrometer scale (Ti-M-4 and Ti-M-5), the TON, initial reaction rate, and also the equilibrium conversion decreased sharply compared to nanoparticles. Therefore, the catalytic activity of Ti-MOR decreases along with the particle length increasing.

The ammoximation is believed to occur in two steps, that is, in situ formation of hydroxylamine via catalytic oxidation of NH<sub>3</sub> by H<sub>2</sub>O<sub>2</sub> on Ti sites and oximation of ketone with hydroxylamine to corresponding oxime [13,16]. Since the second step of oximation is a non-catalytic reaction, it can occur either inside the 12-MR channels of Ti-MOR (Scheme 2A, reaction route I), or in the liquid phase after the hydroxylamine intermediate diffuses out of the zeolite channels (Scheme 2A, reaction route II). Moreover, the intermediate of hydroxylamine is relatively unstable and may undergo decomposition to NO<sub>x</sub> (Scheme 2A, reaction route III). The reaction route I is more favorable than route II for preventing



**Fig. 7.** The catalytic activity of cyclohexanone ammoximation (A) and toluene hydroxylation (B) over various Ti-M samples. Ammoximation conditions: cat., 25 mg; cyclohexanone, 10 mmol; ketone:H<sub>2</sub>O<sub>2</sub>:NH<sub>3</sub> = 1:1.2:1.5 (molar ratio); water, 6 g; temp., 333 K. Hydroxylation conditions: cat., 50 mg; toluene, 10 g; water, 1 g; H<sub>2</sub>O<sub>2</sub> (30 wt.%), 10 mmol; temp., 363 K.



**Scheme 2.** Cyclohexanone ammoximation (A) and toluene hydroxylation (B) over the 12-MR channel of Ti-MOR.

the non-productive decomposition of hydroxylamine, because the cyclohexanone molecules diffusing into the pores would react with hydroxylamine formed therein immediately. Consequently, if the crystal particles become larger, the diffusion distance would be farther for reactants to enter into the 12-MR channels as well as for the intermediates and the products to diffuse out of the channels, and the possible non-productive decomposition for hydroxylamine molecules would increase.

### 3.4.2. Hydroxylation of toluene

The effect of morphology on the catalytic properties of Ti-M was further verified in the hydroxylation of toluene, a reaction needing open spaces. The Ti-M catalyst has already been revealed to be more active than TS-1 zeolite in the hydroxylation of aromatics because of a large porosity of mordenite zeolite [17]. The oxidations are supposed to take place only when the aromatic molecules reach the active sites of Ti peroxo species (Ti-OOH) formed inside zeolite pores.

Fig. 7B exhibits the time course of TON for various Ti-M samples formed. The main products of toluene hydroxylation were the mixture of *o*-cresol, *m*-cresol, and *p*-cresol isomers. The TON of Ti-M-1 (110 nm) was 20 mol (Ti-mol)<sup>-1</sup> at initial 1 h, but the value gradually downgraded to 1 mol (Ti-mol)<sup>-1</sup> for Ti-M-5 (5160 nm) along with the crystal length enlarging. Prolonging the reaction time to 7 h, the TON reached 70.5, 54.7, 44.7, 4.9, and 3.4 mol (Ti-mol)<sup>-1</sup> for Ti-M-1, Ti-M-2, Ti-M-3, Ti-M-4, and Ti-M-5, respectively. Thus, the gap of oxidation activity between different Ti-M samples became more remarkable in the wake of reaction time stretching. The regularity was similar to the abovementioned ammoximation, but the hydroxylation TON disparity among Ti-M-1, Ti-M-2, and Ti-M-3 was larger than that of ammoximation. The 12-MR channels available for catalytic reactions are of one dimensional along the crystal growing direction (*c*-axis). A smaller particle size would shorten the diffusion path for toluene molecules approaching to the Ti sites inside the pores, improving the catalytic performance, as the hydroxylation reaction only occurs over the Ti sites located in the 12-MR channels (Scheme 2B). In addition, the crystal length of *ca.* 1 μm seems to be a demarcation line determining the oxidation activity of Ti-M zeolites: the disparity of activity is small

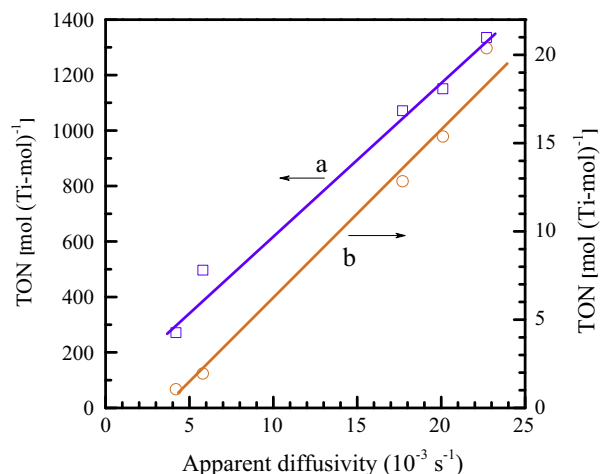


**Fig. 8.** The correlation between apparent diffusivity ( $D/L^2$ ) and TON of cyclohexanone ammoximation (a), and that of toluene hydroxylation (b). The TON was measured at 1 h of reaction time.

within nanometer scale, whereas the activity gap is sharply enlarged when crystals reach micrometer range.

### 3.5. Correlation between oxidation activity and morphology of Ti-MOR

The dependence of relative activity on the crystal length has been investigated (Supplementary Material, Fig. S2). The specific activity (TON) of Ti-M-1 measured at 1 h is assumed to be 100%. The relative activity of cyclohexanone ammoximation and toluene hydroxylation both decreased rapidly with the crystal length becoming longer, especially when the crystal length reached micrometer scale. Another phenomenon observed was that the falling range of relative activity for toluene hydroxylation was larger than that for cyclohexanone ammoximation.

Furthermore, the TON of ammoximation was found to be almost proportional to the apparent diffusivity calculated from the *n*-butane diffusion (Fig. 8a). The same dependence was also observed for the TON of hydroxylation (Fig. 8b). Similar to the

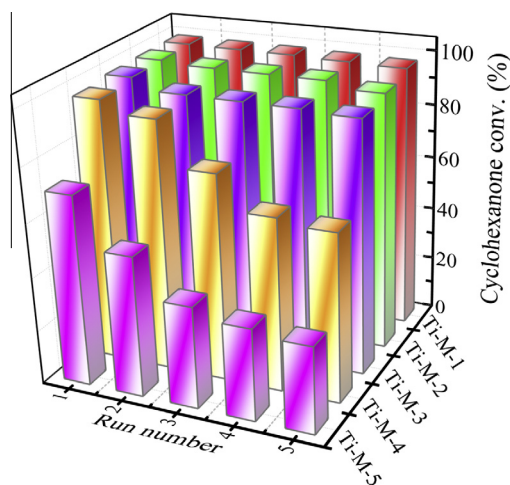


**Fig. 9.** Reusability of Ti-M samples with different morphologies toward the ammoxidation of cyclohexanone in water. Reaction conditions: catalyst:H<sub>2</sub>O:ketone:H<sub>2</sub>O<sub>2</sub>:NH<sub>3</sub> = 0.1 g:6 g:10 mmol:12 mmol:15 mmol; temp., 333 K; 2 h. Regeneration: used catalyst was washed with water and acetone, and dried at 353 K.

result shown in Fig. S2, the TON of toluene hydroxylation decreased more rapidly than ammoxidation with the apparent diffusivity decreasing. That is to say hydroxylation is more sensitive than ammoxidation to the changes of crystal length. This is because that the oxidation could occur either in the 12-MR channels or in liquid phase outside the pores (Scheme 2A); however, the hydroxylation has no option but to occur over the Ti sites in the 12-MR channels (Scheme 2B).

### 3.6. Stability and reusability of Ti-MOR with different morphologies

In addition to catalytic activity, the applicability of titanosilicates depends also on their lifetime and reusability. The reusability of five Ti-M samples has been checked in the ammoxidation of cyclohexanone independently. The experiments were initiated with an enlarged catalyst loading of 0.1 g. The used catalyst was washed with water and acetone, and dried at 353 K. Then, it was subjected to a repeated reaction at a constant ratio of catalyst–substrate–solvent. After five recycles of reaction, nanometer-scaled Ti-M catalysts, namely Ti-M-1, Ti-M-2, and Ti-M-3, maintained the cyclohexanone conversion about 95.0% (Fig. 9). On the contrary, the cyclohexanone conversion decreased to 62.0% from 96.9% and decreased to 32.0% from 70.7% for Ti-M-4 and Ti-M-5, respectively (Fig. 9). Thus, the nanosized Ti-M catalysts were not only more active, but were also more stable than micrometer-scaled ones in batchwise reactions.

The deactivation of titanosilicates in ammoxidation has been previously investigated to be caused mainly by coke formation [40]. Thus, we have characterized the used catalysts. The heavy by-products accumulated gradually with process time and deposited inside the channels of titanosilicates, which may block the Ti active sites wherein. Actually, the TG analysis indicated that the used Ti-M-1 (110 nm) catalysts contained about 5.9 wt.% organic species, which showed a weight loss in a wide temperature range (440–1000 K), including 2.4 wt.% organic species inside channels (Supplementary Material, Fig. S3). We have demonstrated that they corresponded to the heavy by-products formed in ammoxidation system, including cyclohexanecarboxamide,  $\epsilon$ -caprolactam, *N*-cyclohexylidene-cyclohexanamine, and 2-cyclohexylcyclohexanone [18,40]. On the other hand, the weight loss due to organic species reached 7.2 wt.% on the washed Ti-M-5 (5160 nm) catalyst after being used for 5 times, including

4.0 wt.% heavy species inside channels (Supplementary Material, Fig. S3). Thus, the nanosized crystals are helpful to minimize diffusion limitation and suppress coke formation efficiently, which then leads to a longer catalytic life.

## 4. Conclusions

A series of Ti-MOR with different morphologies have been prepared by post-synthesis method, from corresponding aluminosilicates with different degrees of oriented crystal growth along the *c*-axis, the running direction of 12-MR main channels. Smaller particles, especially nanoparticles, are in favor of forming fine tetrahedrally coordinated Ti for shortening the diffusion distance of TiCl<sub>4</sub> vapor molecule inside zeolite micropores. As well, the physicochemical properties and catalytic activity of Ti-MOR zeolites exhibit regular changes with crystal length along the *c*-axis increasing. The hydroxylation of toluene is more sensitive than the ammoxidation of cyclohexanone to the variety of crystal length. The crystal length of ca. 1  $\mu$ m is a remarkable demarcation line governing the adsorption properties and oxidation activity of Ti-MOR. Besides, the catalytic activity of Ti-MOR, which receives double superimposition effects by TiCl<sub>4</sub> vapor treatment and reaction itself, behaves a linear dependence on the apparent diffusivity, for both ammoxidation and hydroxylation.

## Acknowledgments

We gratefully acknowledge the National Natural Science Foundation of China (21373089), the PhD Programs Foundation of the Ministry of Education (2012007613000), and the Shanghai Leading Academic Discipline Project (B409).

## Appendix A. Supplementary material

Supplementary data associated with this article can be found, in the online version, at <http://dx.doi.org/10.1016/j.jcat.2015.03.001>.

## References

- [1] M. Tramasso, G. Perego, B. Notari, US Patent 4410501, 1983.
- [2] G. Bellussi, M.S. Rigguto, *Stud. Surf. Sci. Catal.* 137 (2001) 911–920.
- [3] P. Ratnasamy, D. Srinivas, H. Knözinger, *Adv. Catal.* 48 (2004) 1–169.
- [4] P. Wu, T. Tatsumi, T. Komatsu, T. Yashima, *J. Catal.* 202 (2001) 245–255.
- [5] P. Wu, T. Tatsumi, *Chem. Commun.* (2002) 1026–1027.
- [6] M.A. Cambor, A. Corma, A. Martínez, J. Pérez-Pariente, *J. Chem. Soc. Chem. Commun.* (1992) 589–590.
- [7] P. Wu, T. Komatsu, T. Yashima, *J. Phys. Chem.* 100 (1996) 10316–10322.
- [8] A. Corma, M.T. Navarro, J. Pérez-Pariente, *J. Chem. Soc. Chem. Commun.* (1994) 147–148.
- [9] P. Wu, T. Tatsumi, T. Komatsu, T. Yashima, *Chem. Mater.* 14 (2002) 1657–1664.
- [10] G. Bellussi, C. Perego, in: G. Ertl, H. Knozinger, J. Weiakamp (Eds.), *Handbook of Heterogeneous Catalysis*, vol. 5, Wiley, Poitiers, 1997, p. 2329.
- [11] *Eur. Chem. News* 6 (1995) 23.
- [12] P.R. Saronno, M.P. Milan, et al., US Patent 4745221, 1988.
- [13] P. Roffia, G. Leofanti, A. Cesana, M. Mantegazza, M. Padovan, G. Petrini, S. Tonti, P. Gervasutti, *Stud. Surf. Sci. Catal.* 55 (1990) 43–52.
- [14] C. Neri, B. Anfossi, et al., US Patent 4833260, 1989.
- [15] J.X. Yang, M.K. Yao, S. Zhao, Y.M. Liu, P. Wu, M.Y. He, *Chin. J. Catal.* 31 (2010) 95–99.
- [16] P. Wu, T. Komatsu, T. Yashima, *J. Catal.* 168 (1997) 400–411.
- [17] P. Wu, T. Komatsu, T. Yashima, *J. Phys. Chem. B* 102 (1998) 9297–9303.
- [18] H. Xu, Y.T. Zhang, H.H. Wu, Y.M. Liu, X.H. Li, J.G. Jiang, M.Y. He, P. Wu, *J. Catal.* 281 (2011) 263–272.
- [19] Y.L. Yang, J.H. Ding, B.S. Wang, J. Wu, C. Zhao, G.H. Gao, P. Wu, *J. Catal.* 320 (2014) 160–169.
- [20] J.H. Ding, L. Xu, Y.J. Yu, H.H. Wu, S.J. Huang, Y.L. Yang, J. Wu, P. Wu, *Catal. Sci. Technol.* 3 (2013) 2587–2595.
- [21] J.H. Ding, L. Xu, H. Xu, H.H. Wu, Y.M. Liu, P. Wu, *Chin. J. Catal.* 34 (2013) 243–250.
- [22] W.M. Meier, *Z. Kristallogr.* 115 (1961) 439–450.
- [23] L. Zhang, A.N.C. van Laak, P.E. de Jongh, K.P. de Jong, *Microporous Mesoporous Mater.* 126 (2009) 115–124.
- [24] S. van Donk, J.H. Bitter, A. Verberckmoes, M. Versluijs-Helder, A. Broersma, K.P. de Jong, *Angew. Chem. Int. Ed.* 44 (2005) 1360–1363.

- [25] H. Liu, G.D. Lei, W.M.H. Sachtler, *Appl. Catal. A* 137 (1996) 167–177.
- [26] L. Zhang, S.J. Xie, W.J. Xin, X.J. Li, S.L. Liu, L.Y. Xu, *Mater. Res. Bull.* 46 (2011) 894–900.
- [27] C. Jo, J. Jung, H.S. Shin, J. Kim, R. Ryoo, *Angew. Chem. Int. Ed.* 52 (2013) 10014–10017.
- [28] L. Bonetto, M.A. Camblor, A. Corma, J. Pérez-Pariente, *Appl. Catal. A* 82 (1992) 37–50.
- [29] L.Y. Hu, Z.K. Zhang, S.J. Xie, S.L. Liu, L.Y. Xu, *Catal. Commun.* 10 (2009) 900–904.
- [30] A.J.H.P. van der Pol, A.J. Verduyn, J.H.C. van Hooff, *Appl. Catal. A* 92 (1992) 113–130.
- [31] T. Tatsumi, N. Jappar, *J. Catal.* 161 (1996) 570–576.
- [32] G. Bellussi, M.S. Rigguto, *Stud. Surf. Sci. Catal.* 85 (1994) 177–213.
- [33] K. Segawa, H. Tachibana, *J. Catal.* 131 (1991) 482–490.
- [34] J.T. Miller, P.D. Hopkins, B.L. Meyers, G.J. Ray, R.T. Roginski, G.W. Zajac, N.H. Rosenbaum, *J. Catal.* 138 (1992) 115–128.
- [35] J.C. Groen, W.D. Zhu, S. Brouwer, S.J. Huynink, F. Kapteijn, J.A. Moulijn, J. Pérez-Ramírez, *J. Am. Chem. Soc.* 129 (2007) 355–360.
- [36] C.E. Webster, A. Cottone, R.S. Drago, *J. Am. Chem. Soc.* 121 (1999) 12127–12139.
- [37] D. Lozano-Castello, W. Zhu, A. Linares-Solano, F. Kapteijn, J.A. Moulijn, *Microporous Mesoporous Mater.* 92 (2006) 145–153.
- [38] A. Thangaraj, S. Sivasanker, P. Ratnasamy, *J. Catal.* 131 (1991) 394–400.
- [39] F. Song, Y.M. Liu, H.H. Wu, M.Y. He, P. Wu, T. Tatsumi, *J. Catal.* 237 (2006) 359–367.
- [40] S. Zhao, W. Xie, J.X. Yang, Y.M. Liu, Y.T. Zhang, B.L. Xu, J.G. Jiang, M.Y. He, P. Wu, *Appl. Catal. A* 394 (2011) 1–8.